Journal of Solid State Chemistry 186 (2012) 217–223

Contents lists available at SciVerse ScienceDirect

Journal of Solid State Chemistry

journal homepage: www.elsevier.com/locate/jssc

Photoluminescence and Raman evidence for mechanico-chemical interaction of polyaniline-emeraldine base with ZnS in cubic and hexagonal phase

M. Scocioreanu, M. Baibarac, I. Baltog *, I. Pasuk, T. Velula

National Institute of Materials Physics, Laboratory of Optical Processes in Nanostructured Materials, MG-7, Bucharest-Magurele R77125, Romania

ARTICLE INFO

Article history:
Received 10 September 2011
Accepted 9 December 2011
Available online 17 December 2011

Keywords:
Polyaniline
Zinc sulfide
Raman spectroscopy
Photoluminescence

ABSTRACT

The mechanico-chemical interaction of a polyaniline-emeraldine base (PANI-EB) with ZnS in the cubic and wurtzite phases is studied by Raman spectroscopy and photoluminescence (PL). The results demonstrate that such an interaction leads to the formation of a PANI-salt and metallic Zn. Regardless of the structural form of the ZnS, the formation PANI-salt is indicated by a band in the Raman spectrum that shifts from 1162 to 1176 cm^{-1} and the appearance of a new band at 1330 cm^{-1} that indicates the protonated structure of a PANI-salt. The presence of the second product is determined by comparative PL studies performed on ZnS that has interacted mechanico-chemically with PANI-EB and metallic Zn powder. The variations of the PL spectra and their associated excitation spectra are explained as resulting from the charge collection processes that occur in the composite materials produced by the mechanico-chemical interaction between ZnS and PANI-EB or metallic Zn.

1. Introduction

In the last 20 years, special attention has been given to the luminescence studies of nanostructured semiconductors, such as ZnS, CdS, ZnO and PbI_2. The interest was due to their multiple applications as new displays [1], bio-labels [2], lasers [3] and solar cells [4] for the production of composite materials in which the host matrix are insulating or conducting polymers [5,6]. Inspection of the literature pertaining to ZnS/conducting polymer composite materials reveals that, until recently, polyaniline (PANI) [6] and poly(3-hexylthiophene) [7] were used as the main host macromolecular compounds. At present, two methods are used for the preparation of ZnS/conducting polymers composites: the dispersion of ZnS nanocrystals in polymer solution [7] and the chemical polymerization of the monomer in the presence of ZnS nanoparticles [6]. Another procedure used in this work is to prepare the ZnS/PANI composite by a mechanico-chemical reaction between the ZnS nanometric powder and the polyaniline-emeraldine base (PANI-EB). The mechanico-chemical reaction evolves by a mechanical motion/energy-controlled chemical process [8]. Such a reaction may be produced if the two components in the powder state intensively mixed and subjected to non-hydrostatic compression. The result may be another product, characterized by the occurrence of new chemical bonds between the two components. Such a process is tempting for the production of nanostructured composites when at least one component is a powder consisting of small particles.

For a better understanding of the results presented below, it is necessary to recall several features of the molecular structure of PANI. PANI is a polymer with a repeating unit that contains two parts with different weights (Scheme 1). The reduced ($x=1$) and oxidized ($x=0$) forms are known as leucoemeraldine base (LB) and pernigraniline base (PB), respectively. The intermediate state ($x=0.5$), in which the oxidation and reduction degrees of PANI are equal to each other, is known as PANI-EB. The three forms of PANI correspond to the un-doped state of the polymer. The interaction of PANI with chemical compounds that remove or add electrons from or to the polymer backbone is labeled *p* or *n* doping, respectively. Redox doping transforms the semi-oxidized state (PANI-EB) into a reduced state (PANI-leucoemeraldine) or a fully oxidized state (PANI-pernigraniline). Another way to obtain PANI in a doped state requires acid/base reactions. The three forms of PANI are then labeled as leucoemeraldine salt (LS), emeraldine salt (ES) and pernigraniline salt (PS).

Returning to the problem of semiconducting compounds used as guest nanoparticles in the polymer host matrix, it should be noted that the correlation between the crystallographic structure of semiconductor nanoparticles and their chemical and physical properties has been much debated in recent years. In this context, ZnS must be considered one such material, as it may be produced in two crystallographic structures, cubic and hexagonal. Among the methods used for the synthesis of ZnS particles, both with the cubic (zincblende) and hexagonal (wurtzite) structures the chemical precipitation and annealing treatment in a vacuum at 1050 °C are the most often used.

* Corresponding author. Fax: +40 21 3690177.
E-mail address: ibaltog@infim.ro (I. Baltog).

0022-4596/$ - see front matter © 2011 Elsevier Inc. All rights reserved.
doi:10.1016/j.jssc.2011.12.012

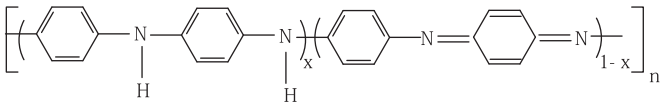

Scheme 1

The goal of this paper is to demonstrate by Raman spectroscopy and photoluminescence studies that the mechanico-chemical reaction between ZnS powder and PANI-EB leads to a new compound in which PANI-EB plays the role of a collector of charges. Such a process results in the transformation of PANI-EB into PANI-salt and the release of metallic Zn. The influence of the two phases of ZnS, i.e., cubic sphalerite and hexagonal wurtzite, on the charge collector property of the ZnS/PANI composite prepared by mechanico-chemical interaction is also evaluated in this paper.

2. Experimental

All chemical compounds used in the synthesis of ZnS and PANI, i.e., $Zn(NO_3)_2$, Na_2S, aniline, $K_2Cr_2O_7$, HCl, NH_4OH, C_2H_5OH, and CH_3CN were purchased from Sigma-Aldrich.

For the synthesis of cubic ZnS, aqueous solutions of Na_2S and $Zn(NO_3)_2$ (both 1 M) were mixed and stirred for 2 min. Afterwards, the mixture was left standing for 30 min. at 25 °C. The resulting white suspension indicated the formation of ZnS. The filtration of the white suspension yielded a filter cake, which was washed with 1000 ml distilled water and 200 ml absolute ethanol to remove residual reactants.

ZnS in the wurtzite crystalline phase was obtained from cubic ZnS after an annealing treatment at 1050 °C in a vacuum of 10^{-5} mbar for 1 h. The crystal structures of the as-grown cubic ZnS powder and wurtzite ZnS were analyzed by X-ray diffraction (XRD) using a Bruker D8 Advance diffractometer with Cu$K\alpha$ radiation.

The PANI was prepared by a typical procedure, in which a mixture of aniline [(1.022 g, 1.09×10^{-2} mol) in 25 ml of 0.5 M HCl] and $K_2Cr_2O_7$ [(0.56 g, 1.9×10^{-3} mol) in 25 ml of 0.5 M HCl] solutions were left standing under ultrasonication for 2 h at 0 °C. The resulting green suspension, which indicated the formation of PANI in its ES form, was filtered, and the filter cake was washed with 1000 ml of deionized water [9]. Afterwards, the washing of the reaction product with 500 ml of 1 M NH_4OH led to the transformation of PANI-ES into PANI-EB. After filtering, the oligomers were extracted with 400 ml CH_3CN until the solvent was colorless, and the remaining powder was dried until it reached a constant mass.

For the preparation of the ZnS/PANI composite, a mechanico-chemical reaction was performed. ZnS powder was mixed with 0.5 and 2 wt% PANI-EB, and the mixtures were compressed non-hydrostatically for 5 min at 0.58 GPa.

Raman studies were carried out at the excitation wavelength of 1064 nm using a FT Raman Bruker RFS 100/S spectrophotometer.

PL spectra, as well as those of PL excitations, were recorded in a right-angle geometry at room temperature using a Horiba Jobin Yvon Flurolog-3 spectrometer, model FL 3-22.

3. Results and discussions

3.1. X-ray diffraction

In Fig. 1, curve a shows three peaks, which appear at 2θ values of 28.9°, 48.3°, and 56.4°, corresponding to the (111), (220), and (311) lattice planes, respectively, which are often reported for cubic ZnS [10]. To determine both the average size of the ZnS crystallites and the microstrain, the XRD data were processed with the MAUD software, version 2.26 [11]. The instrumental line broadening has been evaluated with a heat-treated CeO_2 powder proved to produce no observable size or strain line broadening. Assuming that the crystallites have a spherical shape, a mean size of ~3 nm was obtained. The microstrain, which also contributes to line broadening, was estimated along with the crystallite size. Microstrain values are expressed by the root mean square of the relative variation of the interplanar spacing, $<\varepsilon^2>^{1/2}$, where $\varepsilon=\Delta d/d$ (r.m.s. strain) and d=interplanar distance, which are due to the local distortions of the lattice. Their contribution is evaluated at approximately 4%.

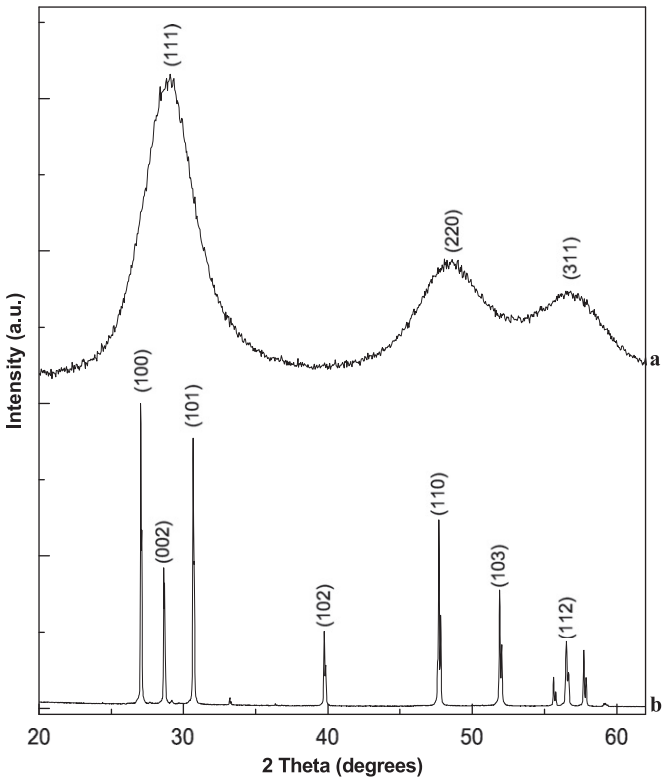

Fig. 1. X-ray spectra of ZnS in cubic (a) and hexagonal phase (b). The latter is obtained from cubic ZnS submitted to 1 h thermal annealing in vacuum at 1050 °C.

The XRD pattern of the hexagonal ZnS obtained by annealing cubic ZnS in a vacuum at 1050 °C for 1 h is shown in Fig. 1, curve b. According to Ref. [12], the strongest peak at $2\theta=27.04°$ observed on spectrum b Fig. 1 corresponds to the [100] diffraction.

3.2. Photoluminescence studies

As is the case for many semiconductor materials in the form of micron- or nano-sized powders, the photoluminescence spectra can be decomposed into several bands that are associated with different radiative recombination processes of the charged carriers produced by band-band irradiation. The situation becomes more complex if one takes into account the different signatures of the recombination processes when they occur in the bulk or at the surface of a particle. In the former case, the excitonic emission and the emission caused by the radiative recombination of charged carriers trapped by vacancies or impurities are dominant, while in the latter case, emission is primarily caused by the involvement of surface states, in which an important contribution comes from the atoms and molecules adsorbed from the

environment. In general, the surface states are generated by dangling bonds that bind by the chemical or physical adsorption of different atoms or molecules from the environment, which subsequently become luminescent centers. In the absorption spectra, the surface states are detected as extended tails toward lower energy than the edge of fundamental absorption band. Usually, the contribution of surface states to the generation of luminescence bands can be modeled by thermal annealing treatments in an advanced vacuum, which results in a decrease of the luminescence intensity and a change of its spectral composition.

Once this framework is established, we can analyze the luminescence spectra of the ZnS powders in two structural forms, cubic and hexagonal, and their changes when composites of ZnS/PANI-EB are produced by mechanico-chemical reactions. Fig. 2 shows the PL spectra of cubic and hexagonal ZnS excited at $\lambda_{exc}=300$ nm. In both cases, the luminescence covers a broad spectral range in which several emission bands can be identified. The PL spectrum of the cubic phase consists of three bands, labeled L_{C1}, L_{C2}, and L_{C3}, with peak at 3.02, 2.61, and 2.15 eV, respectively, i.e., at 410, 475, and 576 nm, while the wurtzite phase discloses only two bands L_{W1} and L_{W2} at 2.7 and 2.38 eV i.e., at 460 and 520 nm. The origin of these emission bands is still a subject under debate. The L_{C1} and L_{C2} emission bands observed for the cubic ZnS are identified with a recombination process associated with sulfur and zinc vacancies, which, as a rule, are luminescent processes occurring in the particle bulk [13,14]. The third L_{C3} band has the characteristics of an emission strongly dependent on the surface state of the particles. Such an explanation is quite possible, taking into account the fact that the entire procedure of synthesis and handling of the final product is done in open atmosphere from which contamination can occur by adsorption of different molecules, the most probable being molecular oxygen. It should be noted that a similar band of high intensity is usually observed in ZnO powders, [15] related to the oxygen molecules trapped by Zn dangling bonds. Fig. 3 supports this reasoning; it shows that an annealing treatment (~200 °C) in a vacuum ($\sim 5\times10^{-5}$ bar) modifies the spectral distribution of the luminescence, the most important change being that of the L_{C3} band, the relative intensity of which decreases faster than the L_{C2} and L_{C1} bands. The change of the emission spectrum is consequently accompanied by a change of the excitation spectrum, which consists of the disappearance of a component located at approximately 3.4 eV. Fig. 3b reveals a typical shape of the excitation spectrum of an indirect gap semiconductor, of which cubic ZnS is an example, which appears as an absorption band that can be decomposed to two components at approximately 3.40 and 2.90 eV. We associate the components at 3.4 and 2.9 eV with two transitions, the former of which is the signature of the volume, which indicates the band gap width, and the latter is the signature of the surface, which indicates the contribution of the tail of states. Such an analysis may lead to the identification of different luminescence mechanisms, with some related to the volume and others to the surface of the particle. In this context, observing the variation of the L_{C3} band in Figs. 3a_1,a_2 in correlation with the associated excitation spectrum (Fig. 3b), the band can be attributed to two luminescence processes. One is produced by the band–band transition at approximately $E_1(L_{C3})\sim3.40$ eV, by which free charge carriers are generated, which may be trapped by Zn or S vacancies. Another portion of the free carriers are trapped by the surface states, where radiative recombination processes occur by irradiation with light of lower energy ($E_2(L_{C3})\sim2.90$ eV) than the gap ($E_2(L_{C3})\sim3.40$ eV), which gives rise to the L_{C3} luminescence band. In the excitation spectra shown in Fig. 3b, the decrease caused by annealing of the E_1 component must be correlated with the decrease of the number of surface traps that results from the annealing vacuum treatment and the resulting desorption of molecules attached to the particle surface.

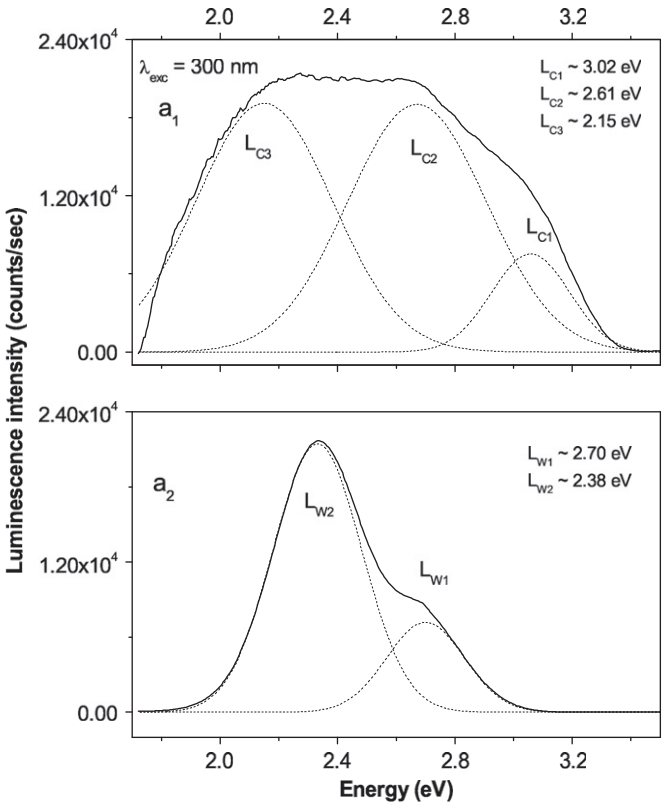

Fig. 2. Emission spectra at room temperature under 300 nm excitation of the ZnS cubic structure as prepared in sample (a_1) and the ZnS in wurtzite structure obtained from cubic ZnS submitted to 1 h thermal annealing in vacuum at 1050 °C (a_2).

Once this analysis framework for the luminescence and excitation spectra is established, the signature of a mechanical–chemical reaction between ZnS and PANI-EB can be identified. For this purpose, Fig. 4a_1, a_2 and b_1, b_2, b_3 are illustrative. The resemblance of the luminescence spectra obtained after annealing in a vacuum (Fig. 2a_2) with those observed on ZnS/PANI-EB composite can immediately be observed. The most important change is the decrease in intensity of the L_{C3} band, which suggests a reduction of the number of radiative recombination processes occurring at the surface of the particles. The decrease in intensity of the L_{C3} band may result from both the reduction of the number of traps able to localize the free charge carriers that occurred in the cubic ZnS after thermal annealing and the reduction of the number of free charge carriers by a charge collecting process that operates in the ZnS/PANI-EB composite. In the latter case, the PANI-EB molecules, which operate as electron traps, are transformed to PANI-ES with the formation of metallic Zn. Fig. 4 reveals a subtle dependence of the emission bands L_{C1}, L_{C2}, and L_{C3} on the excitation spectra with which they are associated. Fig. 4b_1 shows clearly that the L_{C1} emission band is associated with a nearly identical excitation spectrum that consists of only one band, whether it is the spectrum of cubic ZnS alone or that of the ZnS/PANI-EB composite. This means that the L_{C1} band is connected to the volumetric properties that result from radiative recombination processes involving Zn or S vacancies as trapping centers for free carriers generated by the band to band excitation at 3.40 eV. In the excitation spectra associated with the L_{C3} and L_{C2} bands, one finds two components at approximately 3.4 and 3.00 eV, the former indicating a volume property, i.e., a transition that corresponds to the fundamental absorption edge, and the latter a surface property associated with the tail of states.

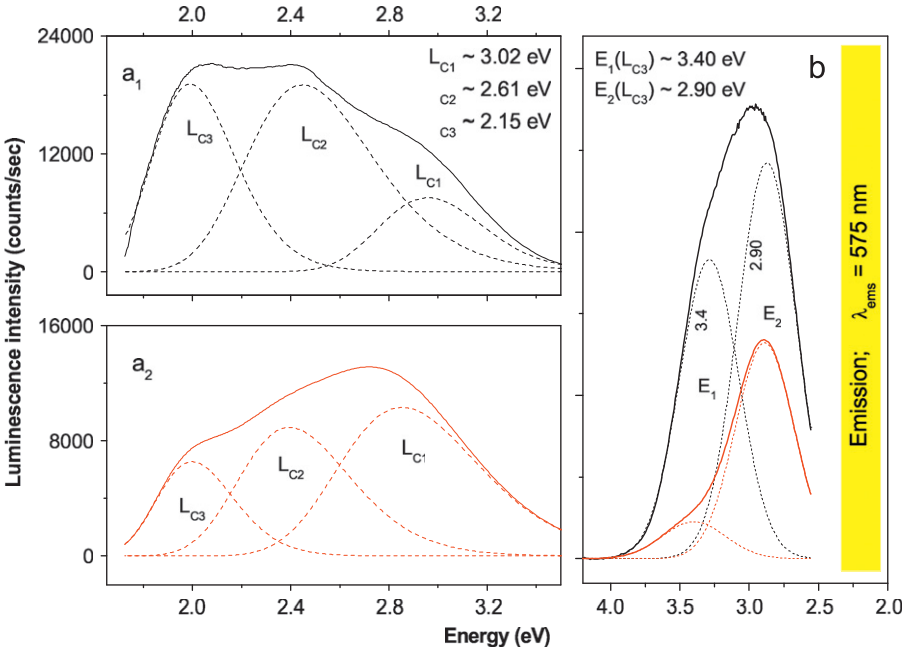

Fig. 3. Emission spectra at room temperature under 300 nm excitation light of the ZnS cubic structures as prepared in sample (a_1) and the same sample after 1 h of thermal annealing in vacuum at 200 °C (a_2). In b are shown the excitation spectra associated with the L_{C3} component of the emission spectrum on the as prepared (black curves) and thermal annealed sample (red curves). (For interpretation of the references to color in this figure, the reader is referred to the web version of this article.)

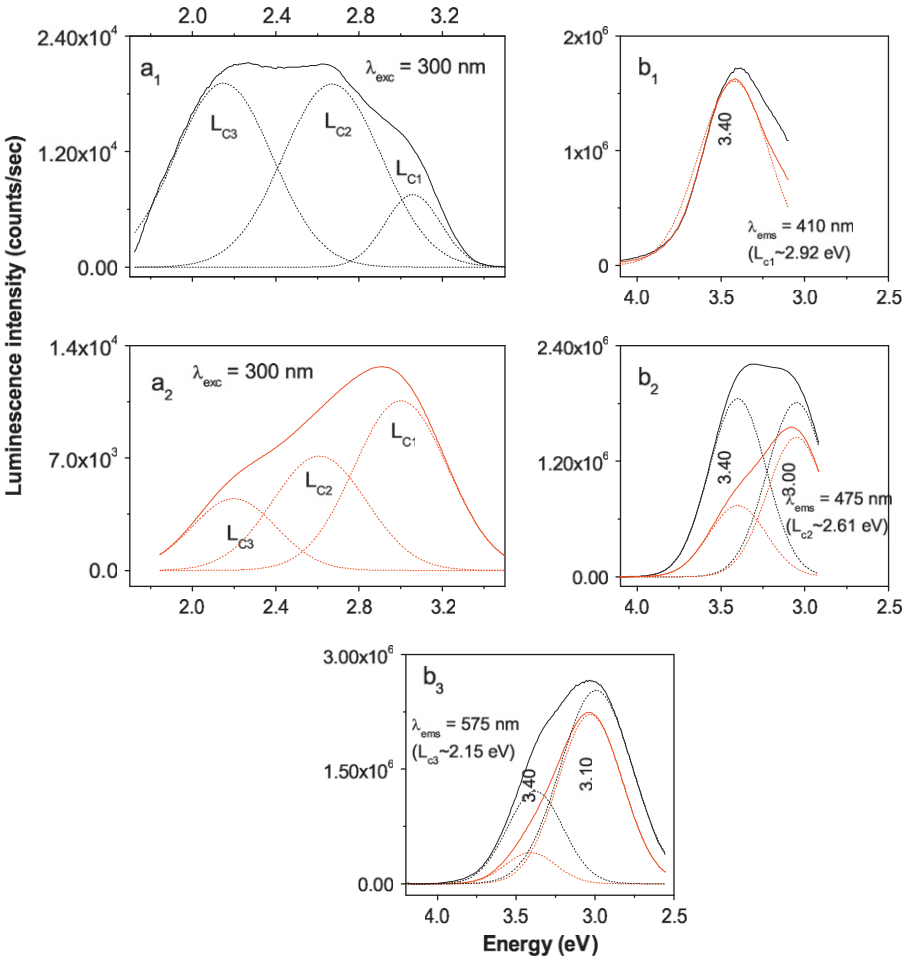

Fig. 4. Emission (a_1, a_2) and excitation (b_1, b_2, b_3) spectra at room temperature under 300 nm excitation of the as prepared cubic ZnS (black curves) and the cubic ZnS compressed non-hydrostatically at 0.58 GPa with 2% PANI-EB (red curves). (For interpretation of the references to color in this figure, the reader is referred to the web version of this article.)

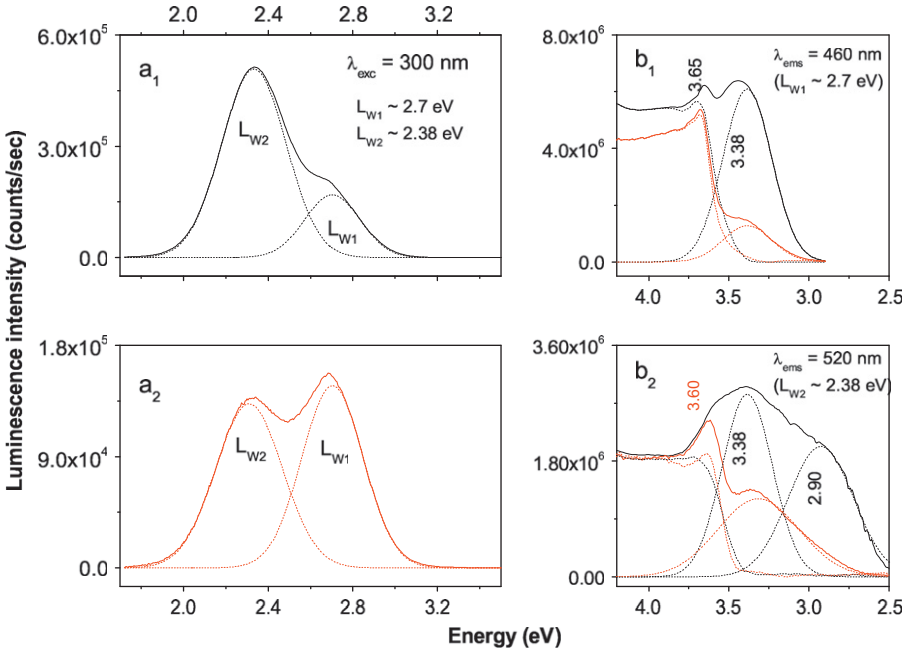

Fig. 5. Emission (a_1, a_2) and excitation (b_1, b_2) spectra at room temperature under 300 nm excitation of the as prepared wurtzite ZnS (black curves) and wurtzite ZnS compressed nonhydrostatically at 0.58 GPa with 2% PANI-EB (red curves). (For interpretation of the references to color in this figure, the reader is referred to the web version of this article.)

Referring to the excitation spectra associated with the L_{C2} and L_{C3} bands, one observes that the efficiency of the excitation at 3.4 eV is greatly diminished in the composite samples, a fact that is explainable by the reduction of free charges by a charge collection mechanism.

If this interpretation is correct, it should also be valid for the explanation of the variation of luminescence spectra of the composites achieved by mechanic-chemical reaction between wurtzite ZnS and PANI-EB. In comparison with the cubic structure, the luminescence spectrum of the wurtzite structure reveals only two emission bands of different intensity, which are labeled L_{W1} and L_{W2} and have maxima at 2.7 eV (~460 nm) and 2.38 eV (~520 nm). *A priori*, invoking a charge collection process, the spectrum should not depend on the crystal structure of ZnS particles. Fig. 5 confirms this. As in Fig. 4, the presence of PANI-EB changes the luminescence of the wurtzite ZnS material by a quenching mechanism that is more active for the L_{W2} emission band. In Fig. 5, it is interesting to observe the shape and variation of the excitation spectra associated with the L_{W1} and L_{W2} bands. The excitation spectra appear as a step, which illustrates the edge of the fundamental absorption band that is always observed as the specific signature of a direct gap semiconductor, such as ZnS in its hexagonal structure. The excitation spectra presented in Fig. 5b_1 and b_2 disclose a band at approximately 3.60 eV that is associated with the band to band transition and two other bands at ~3.38 and ~2.9 eV, which illustrate the contribution of the tails of states. It is interesting that the excitation band at ~2.9 eV is also found in the excitation spectrum associated with the emission bands L_{C3} and L_{C2} from the luminescent spectrum of cubic ZnS. This confirms the earlier statement that the luminescence is generated by excitation in the tails of states and that the tails of states generated by physical and chemical adsorption processes at the particle surface are independent of the crystalline structure. The trapping of free charges at the surface states will be less observable when most of them are collected by PANI-EB. Such a situation is well illustrated in Fig. 5b_1 and b_2 by the red curves.

Summarizing the above results, one can say that in the ZnS/PANI composites produced by mechanico-chemical reactions, regardless of the crystalline structure of ZnS—cubic or hexagonal, the polymer acts as a collector of charges. When the composite is irradiated, that charge collection produces a transition between the valence and conduction bands. This hypothesis is confirmed by Raman scattering studies.

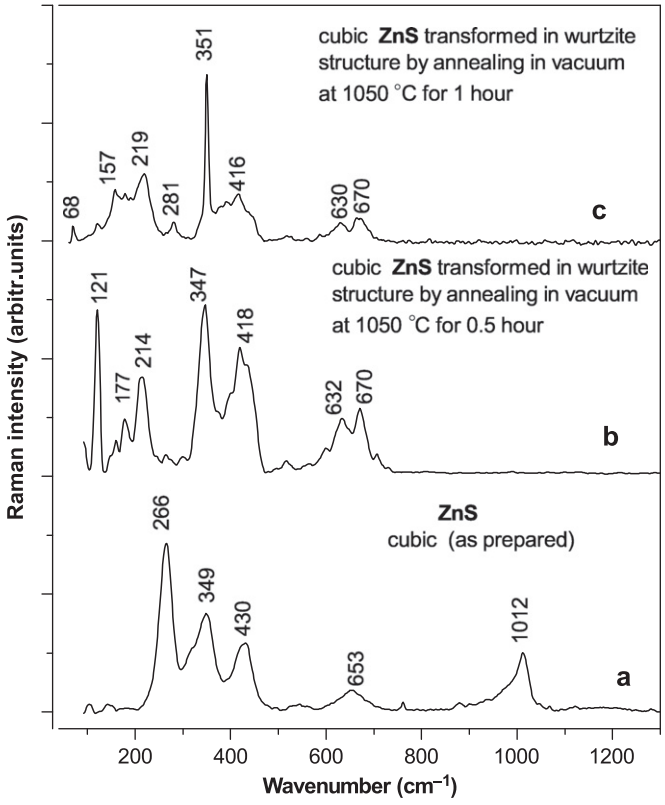

Fig. 6. Raman spectra at λ_{exc}=1064 nm of ZnS particles synthesized in cubic form (curve a) and the same sample transformed to the wurtzite form by a thermal annealing in a vacuum of 10^{-5} mbar at 1050 °C for 0.5 (curve b) and 1 h (curve c).

3.3. Raman spectroscopic studies

Fig. 6 shows the Raman spectra of ZnS in the cubic and hexagonal phases. For the cubic ZnS structure (curve a in Fig. 6), the main Raman lines occur at 266, 349, 430 and 653 cm^{-1}, and they are associated to the following vibrational modes: the transverse optical phonon (TO) at the Γ point, the longitudinal optical phonon (LO) at the Γ point, the TO+longitudinal acoustic phonon (LA), the LO+transverse acoustic phonon (TA) and the second order optical phonon (2LO), respectively [16]. An annealing treatment in a vacuum at 1050 °C for 1 h transforms the cubic ZnS structure into the hexagonal ZnS structure, which is evidenced in the Raman spectrum by the appearance of new bands at 157 cm^{-1} (associated to the disorder-activated (DA) modes), 219 and 416 cm^{-1} (attributed to the first order and second zone-boundary (ZB) phonons), 281 and 351 cm^{-1} ($TO(E_2)$ and $LO(E_1)$ phonons) and 630–670 cm^{-1} (attributed to the second order optical phonon, 2LO) [17,18] (curve c in Fig. 6). An intermediate state obtained during the structural transformation from the cubic to the hexagonal structure is shown in curve b of Fig. 6.

Curves a, b, c and d in Fig. 7 show the Raman spectra of PANI-EB, cubic ZnS, and two ZnS/PANI-EB composites produced by the mechanico-chemical reaction between cubic ZnS and 0.5 and 2 wt% PANI-EB, respectively. Curve e in Fig. 7 shows the Raman spectrum of PANI-ES. According to curve a in Fig. 7, the main Raman lines of PANI-EB are situated at 1162, 1214, 1374, 1486, 1590 and 1610 cm^{-1}, and they are associated with the following

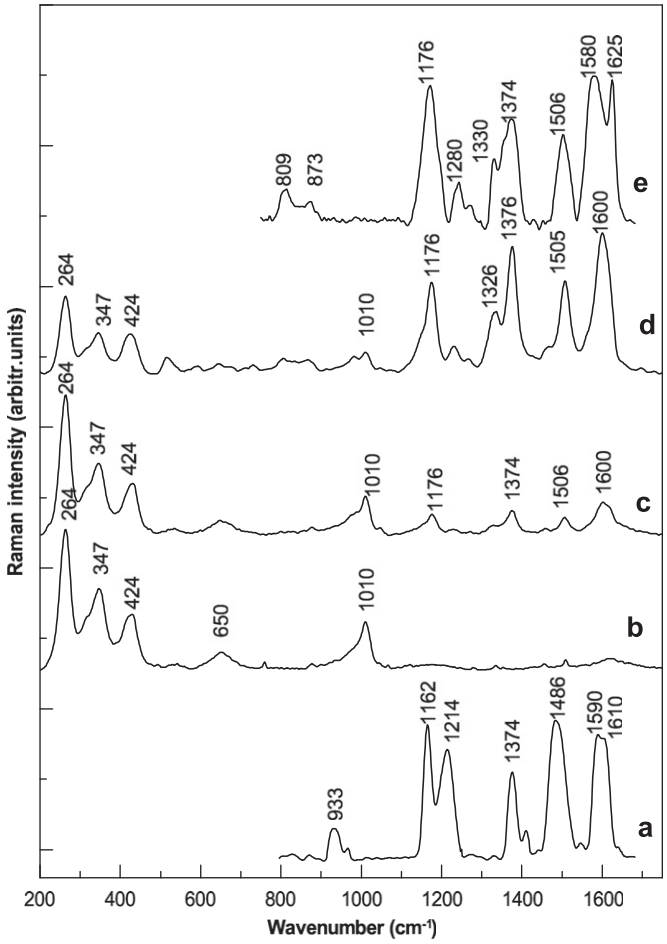

Fig. 7. Raman spectra at λ_{exc}=1064 nm of PANI-EB (a), cubic ZnS (b), the ZnS/PANI composites resulting from the mechanico-chemical reaction (non-hydrostatic compression at 0.58 GPa) between cubic ZnS and PANI-EB at concentrations of 0.5% (c) and 2% (d). Curve e shows the Raman spectra of PANI-ES.

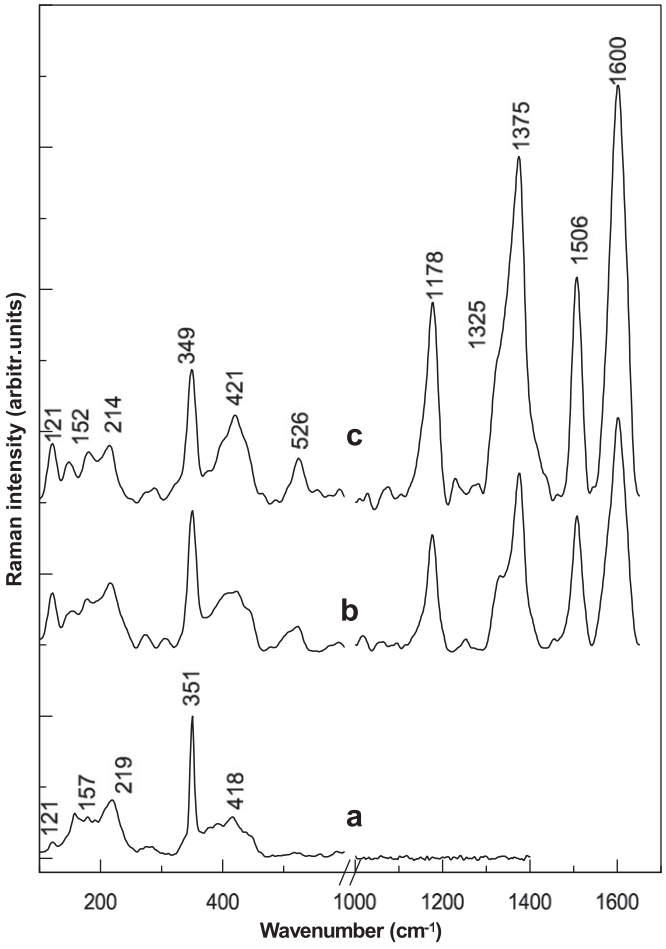

Fig. 8. Raman spectra at λ_{exc}=1064 nm of wurtzite ZnS (a) and ZnS/PANI composites resulting from the mechanico-chemical reaction (non-hydrostatic compression at 0.58 GPa) between wurtzite ZnS and PANI-EB in concentrations of 0.5% (b) and 2% (c).

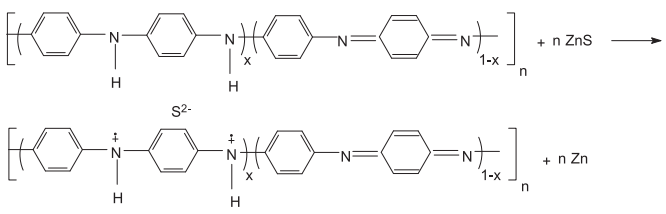

Scheme 2

vibrational modes: C–H bending (quinoide ring (Q)), C–N stretch, C–C stretch, (Q)+C–H bending (B), C=N stretching in the unprotonated segment of quinoide rings, C=C stretch, (Q) and C–C stretch (B) [19,20]. In Fig. 7, curve e shows the Raman lines of PANI-ES situated at 1176, 1240, 1330–1374, 1506, 1580 and 1625 cm^{-1}, whose attribution is to the following vibrational modes: C–H bending (B)-A_g mode, C–C stretch (B)+ring deformation (protonated structure), $C–N^{+}\cdot H–C$ stretch, C=C stretch (Q)+C–C stretch, (B) and C–C stretch, (B)+C–H bending (B), respectively [19,20]. As observed in Fig. 7, independent of the PANI-EB weight used in the mechanico-chemical interaction with the cubic ZnS, the Raman spectra of the ZnS/PANI composite show all vibrational features of PANI-ES. Similar to Fig. 7, Fig. 8 shows the Raman spectra of ZnS in the wurtzite structure (curve a) and of the composites produced by the mechanico-chemical reaction between wurtzite ZnS and PANI-EB at 0.5 and 2 wt% in curves b

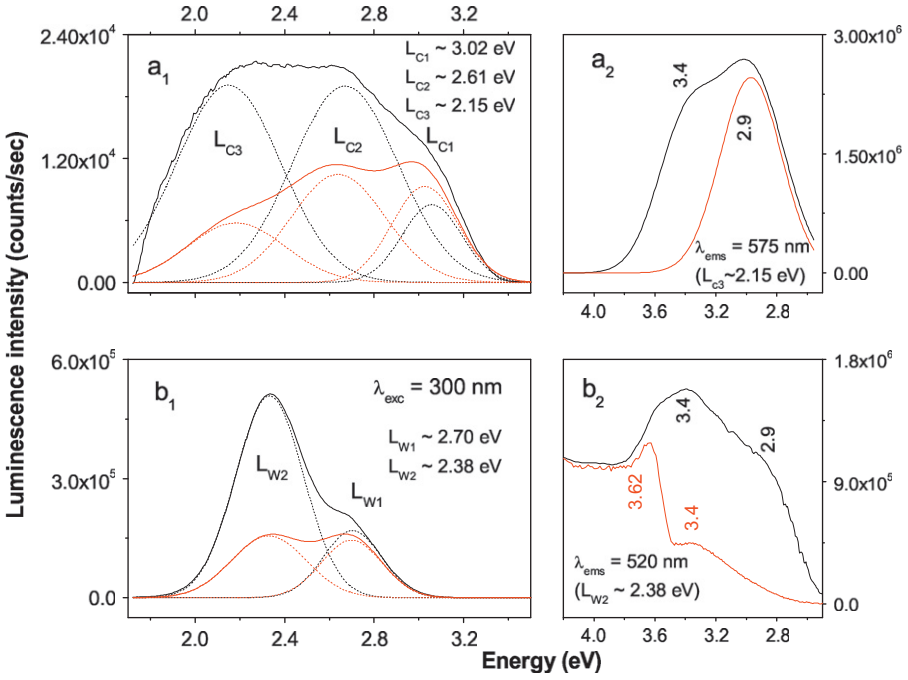

Fig. 9. (a_1). Emission spectra at room temperature under 300 nm excitation light of the as-prepared ZnS sample in cubic structures (black curves) and cubic ZnS interacted with Zn powder under non-hydrostatic compression of 0.58 GPa (red curves). (a_2) The excitation spectra associated with the emission band λ_{ems}=575 nm (L_{C3} ~2.15 eV). (b_1) Emission spectra at room temperature under 300 nm excitation light of the ZnS wurtzite structures obtained after thermal annealing in vacuum at 1050 °C (black curves) and wurtzite ZnS interacted with Zn powder under non-hydrostatic compression of 0.58 GPa (red curves). (b_2). The excitation spectra associated with the emission band λ_{ems}=520 nm (L_{W2}~2.38 eV). (For interpretation of the references to color in this figure, the reader is referred to the web version of this article.)

and c, respectively. As above, in the spectral range from 1000 to 1650 cm^{-1}, the composites show the vibrational features that belong to PANI-ES. These experimental results constitute evidence of a charge transfer between the two constituents that is illustrated by the reaction presented in Scheme 2. The resulting reaction products, according to Scheme 2, correspond to PANI doped with S^{2-} ions, which is understood as a PANI-salt, and metallic Zn. The transformation of PANI-EB into a PANI-salt as a result of the mechanico-chemical interaction of PANI-EB with ZnS is supported in Figs. 7 and 8 by (i) the up-shift of the Raman lines at 1162 and 1486 cm^{-1} to 1178 and 1508 cm^{-1} and (ii) the appearance of the Raman line peaked at 1330 cm^{-1}, which confirms the presence of a protonated structure in the macromolecular chain. The formation of metallic Zn as another reaction product when PANI-EB interacts in a mechanic-chemical reaction with ZnS should induce changes in the PL spectra to those induced when ZnS powder is mixed with metallic Zn. This supposition is verified in Fig. 9, where we find variations similar to those indicated in Figs. 4 and 5. In our opinion, these facts are sufficiently conclusive to argue a process of charge collection that occurs in the ZnS/PANI composites submitted to band to band optical excitation.

4. Conclusions

In this paper, we report new data obtained by Raman scattering and photoluminescence studies on the composites achieved by a mechanico-chemical reaction between ZnS in the cubic or wurtzite phase and PANI-EB. The following results may be highlighted: (i) the mechanico-chemical interaction of PANI-EB with ZnS results in a polyaniline-salt, a fact that is proved by an up-shift of the Raman lines at 1162 and 1486 cm^{-1} to 1178 and 1506 cm^{-1}; (ii) analysis of the excitation spectra and their variation according to the type of ZnS structure has highlighted a charge collection process that occurs under free band-band optical irradiation; and (iii) metallic Zn results from the interaction of ZnS with PANI-EB, and its presence in the ZnS/PANI-EB composite is indicated by similar variations of the mechanico-chemical reaction at 0.58 GPa.

References

[1] J. Hu, L. Li, W. Yang, L. Manna, L. Wang, A.P. Alivisatos, Science 292 (2001) 2060–2063.
[2] M. Kazes, D.Y. Lewis, Y. Ebenstein, T. Mokari, U. Banin, Adv. Mater. 14 (2002) 317–321.
[3] H. Htoon, J.A. Hollingworth, A.V. Malko, R. Dickerson, V.I. Klimov, Appl. Phys. Lett. 82 (2003) 4776.
[4] T. Nakada, M. Hongo, E. Hayashi, Thin Solid Films 242 (2003) 431–432.
[5] L. Zhaang, F. Li, Y. Chen, X. Wang, J. Lumin. 131 (2011) 1701–1706.
[6] K. Dutta, S. Manna, S.K. De, Syn. Metals 159 (2009) 315–319.
[7] M. Mall, P. Kumar, S. Chand, L. Kumar, Chem. Phys. Lett. 495 (2010) 236–240.
[8] K.E. Drexler, Nanosystems: Molecular Machinery Manufacturing and Computation, Wiley, New York, 1992.
[9] M.A. Rodrigues, M.A. de Paoli, M. Mastragostino, Electrochim. Acta 36 (1991) 2143–2146.
[10] M. Mall, P. Kumar, S. Chand, L. Kumar, Chem. Phys. Lett. 495 (2010) 236–240.
[11] L. Lutterotti, Nucl. Instrum. Meth. Phys. Res. B 268 (2010) 334–340.
[12] X. Zhang, Y. Zhang, Y. Song, Z. Wang, D. Yu, Physica E 28 (2005) 1–6.
[13] W.Q. Peng, G.W. Cong, S.C. Qu, Z. Wang, Opt. Mater. 29 (2006) 313–317.
[14] S.K. Mehta, S. Kumar, J. Lumin. 120 (2010) 2377–2384.
[15] M. Baibarac, I. Baltog, T. Velula, I. Pasuk, S. Lefrant, N. Gautier, J. Phys.: Condens. Matter 21 (2009) 445801.
[16] W.G. Nilsen, Phys. Rev. 182 (1969) 838–850.
[17] M. Lin, T. Sudhiranjan, C. Boothroyd, K.P. Loh, Chem. Phys. Lett. 400 (2004) 175–178.
[18] A. Krol, A. Hoffman, J. Gutowski, Phys. Rev. B 38 (1988) 10946.
[19] S. Quillard, G. Louarn, S. Lefrant, A.G. Mac Diarmid, Phys. Rev. B: Condens. Mater. 50 (1994) 12496–12508.
[20] M. Lapkowski, K. Berrada, S. Quillard, G. Louarn, S. Lefrant, A. Pron, Macromolecules 28 (1995) 1233–1238.